Materials Research Bulletin 53 (2014) 145–150

Contents lists available at ScienceDirect

Materials Research Bulletin

journal homepage: www.elsevier.com/locate/matresbu

Dry plasma synthesis of graphene oxide–Ag nanocomposites: A simple and green approach

Yu Wei [a], Xiao Zuo [a], Xuqi Li [b], Shasha Song [a], Longwei Chen [a,*], Jie Shen [a], Yuedong Meng [a], Ying Zhao [b], Shidong Fang [a,*]

[a] Institute of Plasma Physics, Chinese Academy of Sciences, Hefei 230031, China
[b] School of Chemical Engineering, Hefei University of Technology, Hefei 230009, China

ARTICLE INFO

Article history:
Received 28 August 2013
Received in revised form 3 January 2014
Accepted 15 February 2014
Available online 19 February 2014

Keywords:
A. Nanostructure
B. Plasma deposition
C. Electron microscopy

ABSTRACT

A room temperature dry reduction approach, i.e., a low pressure dielectric barrier discharge (DBD) plasma jet, was presented to synthesize highly dispersed graphene oxide-based Ag nanoparticles. TEM, EDS, XRD and XPS tests were used for the characterization of the as-prepared nanocomposites. By comparing the Ag nanoparticles prepared by the DBD plasma jet with and without hydrogen plasma pretreatment, it was found that the latter were highly monodispersed with a uniform size of around 2 nm and deposited on the surface of the graphene oxide as a form of face-centered cubic structure, and it also showed a better antibacterial activity against *Escherichia coli*, which may be due to the smaller particle size, larger surface area and more beneficial dispersity of Ag nanoparticles.

1. Introduction

Great efforts have been made on the fabrication of silver nanoparticles (AgNPs) for many different application purposes such as electronics, optics and catalysis due to their unique electronic, optical and catalytic properties [1,2]. In particular, AgNPs are also shown to be effective biocides against numerous kinds of bacteria, fungi and viruses and therefore attracted considerable attention [3]. AgNPs can cause bacterial cell death by damaging the cell membrane and destroying DNA replication ability [4].

However, the metal NPs can cause aggregation easily, moreover, get deterioration of their antibacterial properties [5]. So it is necessary to find the proper substrates such as carbon fiber and CNTs as the supporter. The metal nanoparticles can be dispersed efficiently by these substrates. Graphene oxide (GO) is one of the most common types of functionalized graphene [6]. It has large surface area as the same as graphene and good water stability, which means that it is a promising candidate for supporting AgNPs. Thus graphene-based composites have aroused extensive interest. Sun' group synthesized graphene oxide–Ag nanocomposites for the molecular sensor [7–10]. Zhang et al. reported a facile one-pot method to synthesize graphene oxide–Ag nanocomposites for surface-enhanced Raman scattering [11]. It is reported that AgNPs retain good antibacterial activity on a GO sheet [12]. A synergistic effect of GO and AgNPs was reported by Ma et al. [13]. Thus the Ag–graphene oxide (Ag–GO) composites are regarded as effective antibacterial materials, which owns the specific properties of both GO and AgNPs.

The traditional methods of preparation of graphene-based AgNPs involve chemical reaction process occurring in solution. Chemical reduction is one of the most popular methods for the preparation of graphene-based AgNPs [14]. The reduction methods usually use chemical agent as reductant, such as hydrazine hydrate and sodium borohydride ($NaBH_4$) [15]. However, the reduction processes usually require high temperature and long reaction time. In addition, surfactants are sometimes used to control particle growth [16]. Although surfactants play an important role in the reaction process, they are pollutant and adverse to the antibacterial property of the composite material. Therefore, the study on the simple and green synthetic method of graphene supported AgNPs composites becomes a necessary and interesting subject. Recently, low-temperature plasma has also been used for the support modification and the metal preparation, which is simpler, greener, milder and more efficient than the conventional methods [17,18]. However, these plasma methods need complicated and expensive equipments such as microwave generators and radio frequency power sources, which limit its further application.

Herein, we reported a simple and green plasma approach to prepare highly dispersed graphene oxide based silver nanoparticles composites, as shown schematically in Fig. 1. These composites were synthesized by an in situ reduction method using graphene oxide sheets as substrates and low-temperature plasma as

* Corresponding authors. Tel.: +86 551 65593308/1380; fax: +86 5515591310.
E-mail addresses: lwchen@ipp.ac.cn (L. Chen), fangsd@ipp.ac.cn (S. Fang).

http://dx.doi.org/10.1016/j.materresbull.2014.02.015
0025-5408/

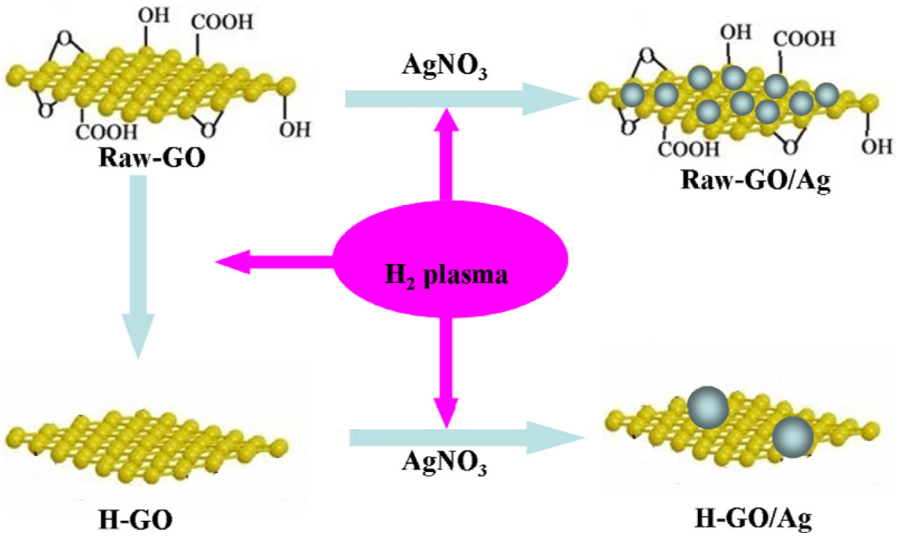

Fig. 1. The mechanism of synthesis of raw-GO/Ag and H-GO/Ag by the dry plasma approach.

reductant. It does not need the solutions and any surfactants. The low-temperature plasma was ignited through another long plasma jet. All the steps were carried out under mild conditions (low temperature and power, around 30 °C and 60 W, respectively). The method is simple, low-cost and environmental friendly, which avoids the use of large amount of chemicals in reduction process and complex equipment such as high frequency power source. The antibacterial performance of the samples is evaluated through inactivation experiments against *Escherichia coli* (*E. coli*).

2. Experimental

2.1. The setup of plasma generator

Fig. 2a and b showed the schematic of the plasma generator and the photograph of the device, respectively. A quartz tube with 6 mm inner diameter is inserted into a cylindrical glass chamber. A copper foil electrode is wrapped around the quartz tube. A 5 kV and 60 kHz sinusoidal voltage (Coronalab power supply, CTP-2000K, China) is applied on the copper foil electrode and a DBD plasma jet is generated through the quartz. Glow plasma is ignited in the bottom of chamber along the surface of substrate by means of the jet. The energy is concentrated in this region where the GO samples are treated.

2.2. Synthesis of Ag–GO nanocomposites

GO was prepared from graphite by the Hummers method. For investigating the effect of hydrogen plasma pretreatment, two kinds of samples were synthesized. The base pressure of the reactor was 5 Pa. The pure H_2 was introduced to the reactor untill the pressure was 20 Pa and soon being ignited. The GO was pretreated for 30 min to get hydrogen plasma pretreatment GO (labeled as H-GO). The GO without any pretreatment is denoted as raw-GO. These two kinds of 100 mg portion of GO powders (i.e., H-GO and raw-GO) were then mixed with the $AgNO_3$ solution (1 mmol/L, 500 ml) and ultrasonically treated 12 h, respectively. Afterward, the mixed solution was dried at 352 K to get powder samples under N_2 conditions. Then these two kinds of powders were reduced by hydrogen plasma for 60 min at the pressure of 10 Pa in order to grow AgNPs on H-GO and raw-GO surface, respectively, Therefore, H_2 reduced H-GO/Ag and raw-GO/Ag materials were synthesized.

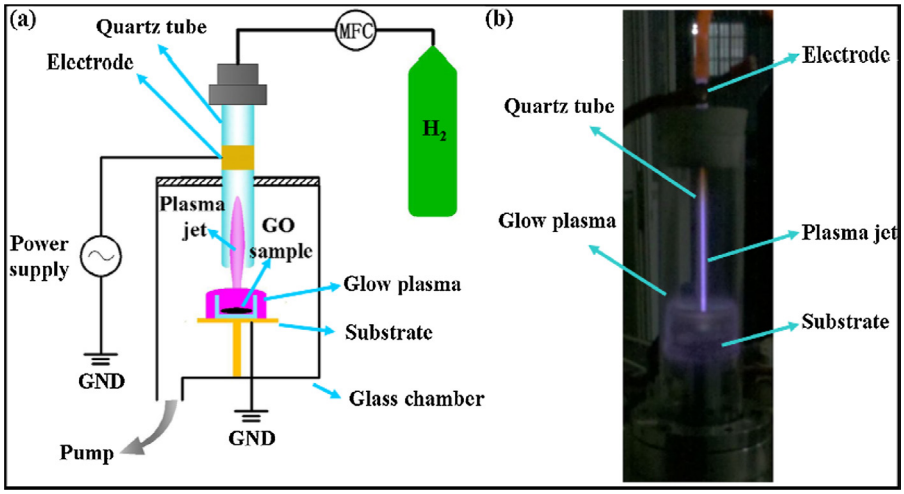

Fig. 2. (a) Schematic of the plasma generator; (b) The photograph of the setup.

2.3. Characterization

JEM-2100F transmission electron microscope (TEM) was used to examine the morphology of the composites. Energy dispersive X-ray spectroscopy (EDS) was used to detect the distribution of element of the composites. X-ray diffraction (XRD) was carried out on Philips X'Pert G2234 XRD system with Cu Kα radiation and scanning in the range of 10–80°. X-ray photoelectron spectroscopy (XPS) studies were performed on a Thermo ESCALAB250 photoelectron spectrometer.

2.4. Antibacterial evaluation

The antibacterial activity test against *E. coli* was evaluated using the disk diffusion test and shake flask test. Before microbiological experiments, all glassware and culture media were sterilized by autoclaving at 393 K for 15 min. In the disk diffusion test, the plates were filled with agar medium and then were inoculated. The bacteria were diluted to 10^6 colony forming units (CFU) mL^{-1}. The diluted *E. coli* was spread on the culture media in the Petri dish, and then laid the samples. The zone of inhibition was recorded after 24 h of nurture at 37 °C. In the shake flask test, 50 ml of saline solution inoculating with *E. coli* was taken for having 10^6 cells in the flask. Afterwards, 50 mg of H-GO/Ag and raw-GO/Ag composites were added to it, respectively. Then both them were stirred at room temperature. The number of surviving *E. coli* was tested by the plate colony count method.

3. Result and discussion

3.1. Structure characterization

Fig. 3 shows the typical TEM images of the two samples. It can be seen that the folds of GO sheets and AgNPs decorated on them. The images of these two samples show highly dispersed AgNPs on raw-GO surface and a greater agglomeration of H-GO/Ag composites. As shown in Fig. 3b, AgNPs are highly dispersed on raw-GO surface with uniform size of around 2 nm. In contrast, AgNPs on H-GO surface show a higher degree of aggregation (Fig. 3a). From Fig. 3a we can see that most of the particle radiuses exceed 10 nm. It means that the morphology and size of the AgNPs can be controlled via the hydrogen plasma pretreatment of GO. The HRTEM images and corresponding FFT analysis (Fig. 3c and d) of AgNPs indicate that they are crystalline. The interplanar spacing of the particle lattice is 0.23 nm, which corresponds to the (1 1 1) lattice plane of Ag. The Fig. 4a and b confirms the existence of AgNPs. The EDS elemental mapping further indicates that the Ag–GO composites are successfully synthesized (Fig. 4c and d). The white and red color dots denote carbon and Ag, respectively. Corresponding element mapping images show that the outline of Ag element is almost the same as the outline of C element, indicating the uniform distribution of AgNPs on the raw-GO surface.

To further validate the AgNPs anchored onto the GO sheets and to valuate the mass ratio of Ag/GO, XRD (X-ray diffraction) and XPS (X-ray photoelectron spectroscopy) are applied in measurements. Fig. 5 shows the XRD patterns of raw-GO sheets and raw-GO/Ag composites. The curve of GO sheets shows a diffraction peak at a 2θ value around 11.4°, which may be due to interlamellar water trapped between hydrophilic graphene oxide sheets [19]. In the curve of raw-GO/Ag composites, the clear peaks at 2θ values of about 38.1°, 44.3°, 64.5° and 77.5° are assigned to the Ag(1 1 1), Ag (2 0 0), Ag(2 2 0), and Ag(3 1 1), respectively. The crystallite size of AgNPs on GO sheets is calculated to be 2.4 nm, which is in good agreement with the results of TEM. This result indicates that the AgNPs have successfully located onto the GO surface as a form of face-centered cubical (fcc) structure, and has no changes in the crystalline structures after the treatment of hydrogen plasma. The peak of GO are not found in the raw-GO/Ag composites, because the regular stack of GO is destroyed by the intercalation of AgNPs [20,21]. From the XRD analysis, we can see that the hydrogen plasma can transform the metal ion precursor into metal nanocrystal and cause damage to the graphene network.

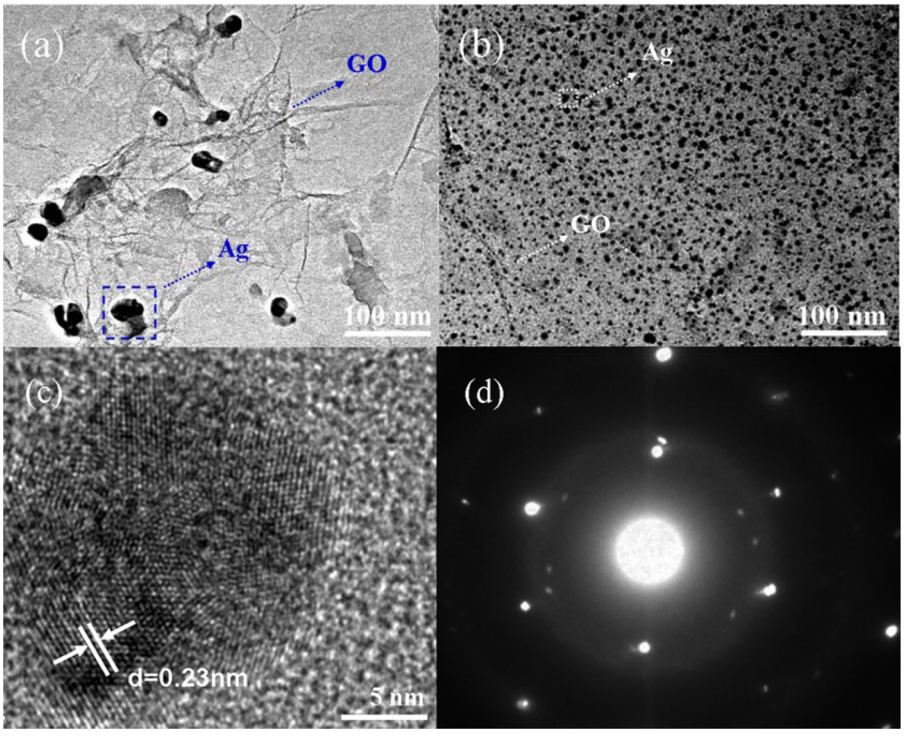

Fig. 3. TEM images of (a) H-GO/Ag; (b) raw-GO/Ag; (c) HRTEM images of AgNPs and (d) corresponding FFT analysis.

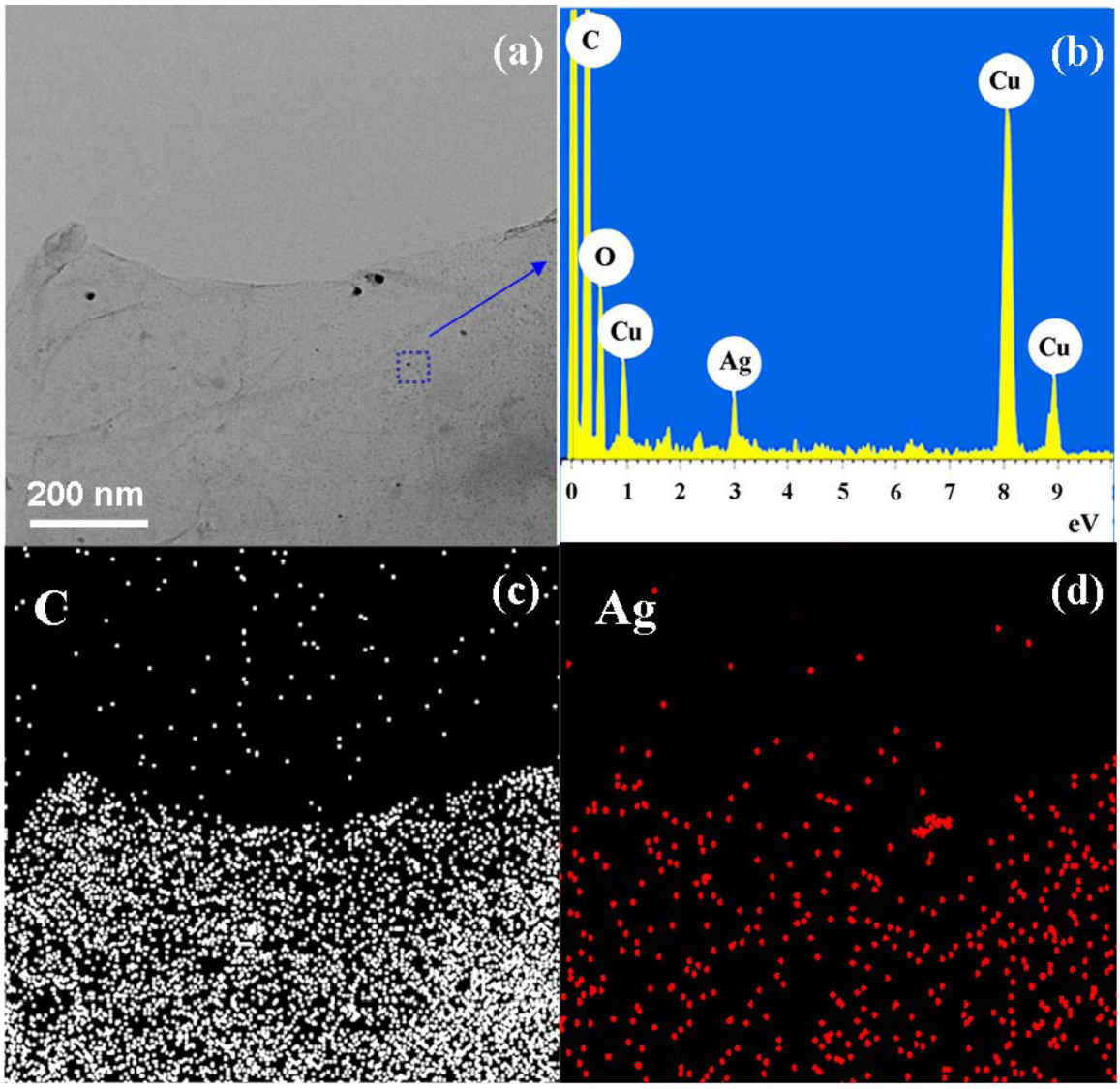

Fig. 4. (a) TEM image of raw-GO/Ag; (b) EDS pattern of raw-GO/Ag; (c) The carbon elemental mapping of raw-GO/Ag; (d) The silver elemental mapping of raw-GO/Ag.

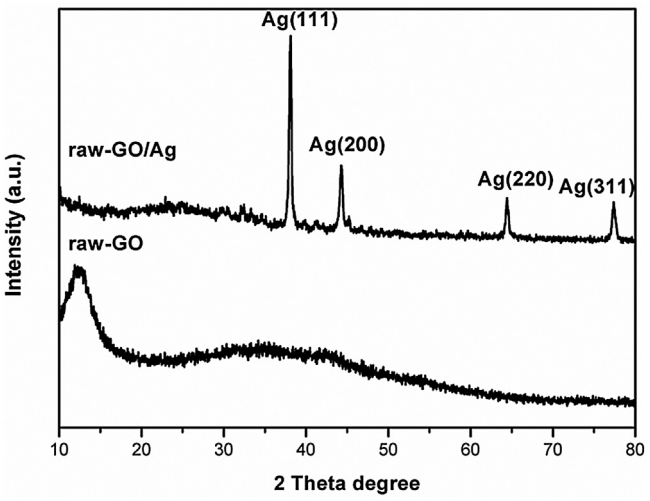

Fig. 5. XRD patterns of raw-GO and raw-GO/Ag.

The XPS spectrum of raw-GO/Ag composites in Fig. 6 shows that the major element peaks belong to C 1s, O 1s and Ag 3d, respectively. The percentage by weight of each element is shown in the inset of Fig. 6. The percentage by weight of AgNPs in raw-GO/Ag composites is 22.28%, illustrating the mass ratio of Ag/GO is about 1/4, which is less than the ratio of H-GO/Ag composites. From the inset of Fig. 6, we can also see that the percentage by weight of oxygen in H-GO/Ag composites is less than that in raw-GO/Ag composites. This may be due to the reduction of oxygen groups and the plasma etching effect occurring in the hydrogen pretreatment process. The reduced O species in H-GO/Ag indicate that some of the oxygen functional groups have indeed been removed by pre-hydrogen treatment, and induce the poor dispersion of AgNPs.

According to the above results, it is evident that the plasma treatment and the oxygen functional groups play an important role on the nucleation of AgNPs. The mechanisms of AgNPs formation under plasma exposure involve two processes. Firstly, the Ag precursor ($AgNO_3$) mixed with GO is diluted by water and ultrasonically treated for 12 h. With the evaporation of water, the $AgNO_3$ concentration becomes higher and higher to a critical point at which Ag precursor crystallizes on the GO. The Ag precursor

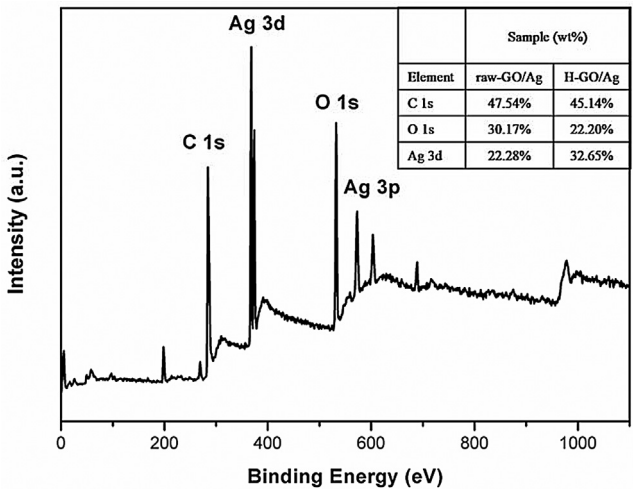

	Sample (wt%)	
Element	raw-GO/Ag	H-GO/Ag
C 1s	47.54%	45.14%
O 1s	30.17%	22.20%
Ag 3d	22.28%	32.65%

Fig. 6. XPS spectra of raw-GO/Ag.

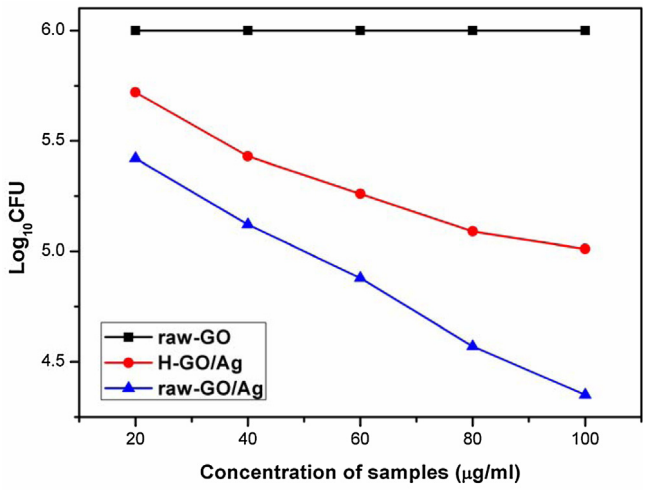

Fig. 8. Antibacterial activity of raw-GO, H-GO/Ag and raw-GO/Ag composites at different concentration and with the initial *E. coli* concentration of 10^6 CFU mL^{-1}.

crystallizes homogeneously on the surface of GO supporters. Secondly, the samples are treated by the dry hydrogen plasma. Several types of ions (H^+ and H^-), excited atoms and molecules and electrons are the major particles in the hydrogen plasma [22]. H ions, H atoms, and electrons can effectively reduce the metal precursors to the metallic species at room temperature. Because the dry hydrogen plasma used is mild plasma, there is not enough energy from the plasma, and as a result the Ag precursor cannot be evaporated. In the meantime, the electrons get enough energy that they are trapped by the Ag+ ions, which are then transformed into Ag atoms. The Ag atoms move at the GO surface and find the places where the potential energy is lower and then crystallize at the anchoring point. The crystals will grow larger and larger over time. So Ag crystallite nucleates on GO surface. In our discharging device, the plasma is concentrated in the bottom of chamber where the GO samples are treated. NO energy is wasted, which means it is a green and high-efficiency method.

According to the research published by Faria et al. [23], the presence of oxygenated groups has great influence on the associated kinetic process of AgNPs deposition. The oxygenated groups on the surface of GO sheets provide possible nucleation sites for anchoring of the AgNPs [24]. The AgNPs showed an apparent size-dependent tendency toward narrower distributions when presence of oxygenated groups, which can lead to surface stabilization and suppress the growth of nanoparticles [23]. This conclusion is highly identical with ours.

3.2. Study on the antibacterial effects

Two kinds of test were carried out for assessing the antibacterial activities of the raw-GO/Ag composites, H-GO/Ag and the control sample of raw-GO without any treatment.

In the disk diffusion test, the antibacterial effects were reflected by the size of inhibition zones (Fig. 7). The mass of each sample is 5 mg. Except for the control sample, all as-prepared Ag–GO composites exhibit relatively strong antibacterial activity which can be known from the inhibition zone, indicating that the AgNPs give the most contribution to the antibacterial activities of the composites. The radius of inhibition zone is 3.1 cm and 5.2 cm for H-GO/Ag and raw-GO/Ag composites, respectively. The result reveals that the raw-GO/Ag containing smaller aggregates has greater antibacterial activity even with a lower mass percentage of Ag compared to the H-GO/Ag composites. Das et al. reported that the antibacterial activity of AgNPs on GO sheets is size and shape dependent. The toxicity of AgNPs is size dependent and the smaller sized nanoparticles exhibit higher antibacterial activity, which was attributed to the high specific surface area and easy cell penetration [3]. Therefore, the raw-GO/Ag composites with a uniform distribution of AgNPs with diameters around 2 nm prepared by the low temperature dry plasma are expected to be promising antibacterial material.

Shake flask test was done for raw-GO/Ag and H-GO/Ag composites by the measurement of surviving cells under the treatment of Ag-GO composites through CFUs. The CFUs of the

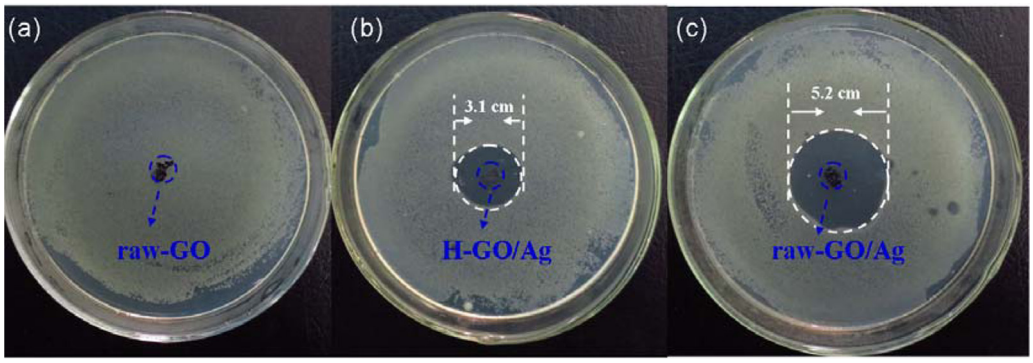

Fig. 7. Optical images of the zone of inhibition for (a) raw-GO (b) H-GO/Ag (c) raw-GO/Ag.

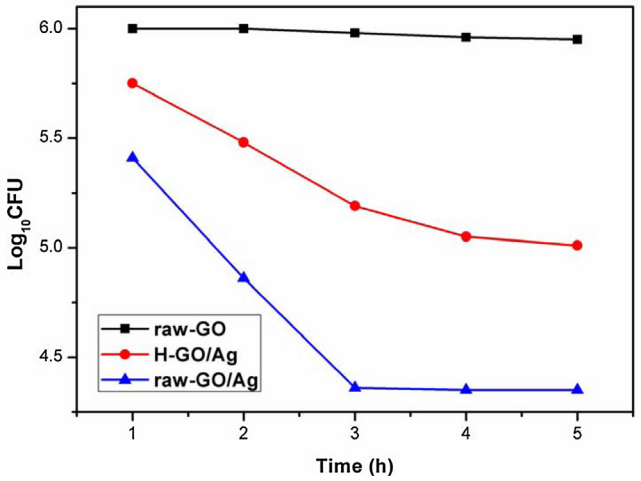

Fig. 9. Antibacterial activity of raw-GO, H-GO/Ag and raw-GO/Ag composites at different time with the initial *E. coli* concentration of 10^6 CFU mL^{-1}.

surviving *E. coli* after exposure to Ag–GO composites at different concentration for various times are shown in Fig. 8 and Fig. 9. The results indicate that both raw-GO/Ag and H-GO/Ag have high-performance antibacterial capability at relatively low concentration. It can be seen in Fig. 9 that at the same concentration, raw-GO/Ag composites illustrate the highest disinfection rate compared to H-GO/Ag composites. The cells were killed completely within 3 h when the concentration of raw-GO/Ag composites was 100 μg mL^{-1}. These results further confirmed that raw-GO/Ag composites had enhanced antibacterial activity. Compared to H-GO/Ag composites, the raw-GO had almost no antibacterial activity. However, future studies on the biocidal influence of these materials on other Gram-negative and Gram-positive bacteria are necessary to adequately evaluate its possible use as a new antibacterial material.

4. Conclusions

In summary, Ag–GO antibacterial materials were prepared by a simple and green route using dry plasma technique. The results demonstrated that the as-synthesized Ag–GO composites displayed effective antibacterial activity against *E. coli*. And the raw-GO/Ag composites containing smaller aggregates have greater antibacterial activity than that of the H-GO/Ag composites. The simple, green and in-situ synthesis is a promising alternative to prepare Ag–GO antibacterial materials.

Acknowledgment

This work is financially supported by the National Natural Science Foundation of China under Grant Nos. 11205201, and 21377133.

Reference

[1] Y.G. Sun, Y.N. Xia, Science 298 (2002) 2176–2179.
[2] R. Pasricha, S. Gupta, A.K. Srivastava, Small 5 (2009) 2253–2259.
[3] C. Marambio-Jones, E.M.V. Hoek, Journal of Nanoparticle Research 12 (2010) 1531–1551.
[4] I.V. Lightcap, T.H. Kosel, P.V. Kamat, Nano Letters 10 (2010) 577–583.
[5] J.F. Shen, M. Shi, N. Li, B. Yan, H.W. Ma, Y.Z. Hu, M.X. Ye, Nano Research 3 (2010) 339–349.
[6] J.Z. Ma, J.T. Zhang, Z.G. Xiong, Y. Yong, X.S. Zhao, Journal of Materials Chemistry 21 (2011) 3350–3352.
[7] S. Liu, J.Q. Tian, L. Wang, X.P. Sun, Carbon 49 (2011) 3158–3164.
[8] S. Liu, L. Wang, J.Q. Tian, Y.L. Luo, X.X. Zhang, X.P. Sun, Journal of Colloid and Interface Science 363 (2011) 615–619.
[9] S. Liu, J.Q. Tian, L. Wang, H.L. Li, Y.W. Zhang, X.P. Sun, Macromolecules 43 (2010) 10078–10083.
[10] Y.W. Zhang, S. Liu, L. Wang, X.Y. Qin, J.Q. Tian, W.B. Lu, G.H. Chang, X.P. Sun, RSC Advances 2 (2012) 538–545.
[11] Z. Zhang, F.G. Xu, W.S. Yang, M.Y. Guo, X.D. Wang, B.L. Zhanga, J.L. Tang, Chemical Communications 47 (2011) 6440–6442.
[12] K.C. Song, S.M. Lee, T.S. Park, B.S. Lee, Korean Journal of Chemical Engineering 26 (2009) 153–155.
[13] K.J. Jeon, Z. Lee, Chemical Communications 47 (2011) 3610–3612.
[14] Z. Zhang, J. Zhang, B.L. Zhang, J.L. Tang, Nanoscale 5 (2013) 118–123.
[15] J. Liu, Z.Q. Jiang, Z.J. Jiang, Y.D. Meng, Journal of Materials Chemistry 21 (2011) 5565–5568.
[16] Z.C. Liu, C.F. Yu, I.A. Rusakova, D.X. Huang, P. Strasser, Topics in Catalysis 49 (2008) 241–250.
[17] K. Kamataki, H. Miyata, K. Koga, G. Uchida, N. Itagaki, M. Shiratani, Applied Physics Express 4 (2011).
[18] Q. Wang, M.M. Song, C.L. Chen, Y. Wei, X. Zuo, X.K. Wang, Applied Physics Letters 101 (2012).
[19] S. Park, J.H. An, I.W. Jung, R.D. Piner, S.J. An, X.S. Li, A. Velamakanni, R.S. Ruoff, Nano Letters 9 (2009) 1593–1597.
[20] M.R. Das, R.K. Sarma, R. Saikia, V.S. Kale, M.V. Shelke, P. Sengupta, Colloids and Surfaces B: Biointerfaces 83 (2011) 16–22.
[21] X.Q. Fu, F.L. Bei, X. Wang, S. O'Brien, J.R. Lombardi, Nanoscale 2 (2010) 1461–1466.
[22] J.H. He, I. Ichinose, T. Kunitake, A. Nakao, Langmuir 18 (2002) 10005–10010.
[23] A.F. Faria, D.S.T. Martinez, A.C.M. Moraes, M.E.H.M. da Costa, E.B. Barros, A.G. Souza, A.J. Paula, O.L. Alves, Chemistry of Materials 24 (2012) 4080–4087.
[24] Z.J. Wang, X.Z. Zhou, J. Zhang, F. Boey, H. Zhang, The Journal of Physical Chemistry C 113 (2009) 14071–14075.